Naval Research Laboratory

Washington, DC 20375-5320

NRL/MR/5317--20-10,131

Cylindrical Array Radar: Comparison to Multi-Faced Systems for Horizon Surveillance and Application to Ubiquitous Radar

W. Mark Dorsey

Radar Analysis Branch
Radar Division

September 29, 2020

REPORT DOCUMENTATION PAGE

Form Approved
OMB No. 0704-0188

1. REPORT DATE *(DD-MM-YYYY)*	**2. REPORT TYPE**	**3. DATES COVERED** *(From - To)*
29-09-2020	NRL Memorandum Report	10/1/2019 – 07/29/2020

4. TITLE AND SUBTITLE

Cylindrical Array Radar: Comparison to Multi-Faced Systems for Horizon Surveillance and Application to Ubiquitous Radar

5a. CONTRACT NUMBER

5b. GRANT NUMBER

5c. PROGRAM ELEMENT NUMBER
62271N

6. AUTHOR(S)

W. Mark Dorsey

5d. PROJECT NUMBER

5e. TASK NUMBER

5f. WORK UNIT NUMBER
6B10

7. PERFORMING ORGANIZATION NAME(S) AND ADDRESS(ES)

Naval Research Laboratory
4555 Overlook Avenue, SW
Washington, DC 20375-5320

8. PERFORMING ORGANIZATION REPORT NUMBER

NRL/MR/5317--20-10,131

9. SPONSORING / MONITORING AGENCY NAME(S) AND ADDRESS(ES)

Office of Naval Research
One Liberty Center
875 N Randolph Street, Suite 1425
Arlington, VA 22203-1995

10. SPONSOR / MONITOR'S ACRONYM(S)
ONR

11. SPONSOR / MONITOR'S REPORT NUMBER(S)

12. DISTRIBUTION / AVAILABILITY STATEMENT

DISTRIBUTION STATEMENT A: Approved for public release; distribution is unlimited.

13. SUPPLEMENTARY NOTES

14. ABSTRACT

Cylindrical phased arrays are an attractive aperture for radar applications due to their steering-angle independent gain, beamwidth, polarization, sidelobe levels, and reflection coefficient. Moreover, the ease with which they form omnidirectional and wide--sector--covering transmit beams facilitates ubiquitous radar -- allowing the ability to simultaneously see everywhere. The reduced scan time of ubiquitous radar, however, is coupled with an increased dwell time to maintain constant range. In this report, we investigate the benefits that a cylindrical array can offer to a radar system -- both for standard surveillance radar and ubiquitous approaches.

15. SUBJECT TERMS

Surveillance Radar Circular Array

16. SECURITY CLASSIFICATION OF:			**17. LIMITATION OF ABSTRACT**	**18. NUMBER OF PAGES**	**19a. NAME OF RESPONSIBLE PERSON**
					W. Mark Dorsey
a. REPORT	**b. ABSTRACT**	**c. THIS PAGE**	Unclassified Unlimited	29	**19b. TELEPHONE NUMBER** *(include area code)*
Unclassified Unlimited	Unclassified Unlimited	Unclassified Unlimited			(202) 404-5639

Standard Form 298 (Rev. 8-98)
Prescribed by ANSI Std. Z39.18

UNCLASSIFIED//DISTRIBUTION A

This page intentionally left blank.

CONTENTS

This page intentionally left blank.

CYLINDRICAL ARRAY RADAR

1. Executive Summary

Cylindrical phased arrays are an attractive aperture for radar applications due to their steering-angle independent gain, beamwidth, polarization, sidelobe levels, and reflection coefficient. Moreover, the ease with which they form omnidirectional and wide–sector–covering transmit beams facilitates ubiquitous radar – allowing the ability to simultaneously see everywhere. The reduced scan time of ubiquitous radar, however, is coupled with an increased dwell time to maintain constant range. In this report, we investigate the benefits that a cylindrical array can offer to a radar system – both for standard surveillance radar and ubiquitous approaches.

2. Introduction

Small platforms play a pivotal role in the modern Navy by performing the forward sensing required to extend the *eyes and ears* of larger platforms. Efficient surveillance radar is a necessity enabling these platforms to sense their environment. Trunk and Patel investigated the optimal configuration for a multi-faced array-based surveillance radar. Initial studies focused on horizon surveillance and used the relative horizon search time as the defining metric [1, 2]. In these and subsequent studies, they assumed transmit/receive (T/R) modules were distributed equally throughout the array. The benefits offered by simultaneously using multiple array faces were discussed. However, no mention was made of the benefits obtained when using multiple faces coherently. The initial studies concluded that the optimal number of faces is three – a finding reinforced by a later study performed by Waters on volume surveillance [3]. Trunk took a fresh look at this concept again in 2003 that included a redefined representation of scan loss along with the impact of clutter fill pulses [4]. Here, Trunk concluded that the reduction in scan positions offered by a four-face system proved optimal.

The concept of ubiquitous radar is to look everywhere, all the time – a concept that is seen as a way of providing the persistent awareness desired by small Navy platforms. In ubiquitous radar systems, a broad transmit beam illuminates a large surveillance volume that is then tiled with many (ideally) simultaneous, contiguous, high-gain receive beams. This continuous illumination allows increased integration time to make up for the decrease in sensitivity resulting from a low gain transmit beam [5]. This radar concept, seen as a futuristic capability as recently as 2002 [6], is now more realizable thanks to advances in digital beamforming (DBF). The concept of ubiquitous radar was initially discussed using planar arrays, however key limitations are presented by planar arrays that limit the effectiveness of the radar technique [5]. Synthesizing broad transmit patterns without severely limiting effective radiated power (ERP) is a challenging problem with planar arrays. Techniques have been developed [7–9], but even those cover an angular sector of only moderate width.

Circular/cylindrical apertures overcome many of the challenges presented by planar arrays to a ubiquitous radar system. Transmitting with omnidirectional patterns – or broad, sector–covering patterns – is

Manuscript approved September 25, 2020.

straightforward with appropriately designed circular apertures. Directional radiation patterns may also be formed and steered over a full 360° without significant changes to pattern shape, sidelobe structure, or polarization. The width of the sector and beamwidth of directional beams are reconfigured with ease, thus providing variation on the effective size of the transmit/receive faces. These advantages make cylindrical apertures preferable, in principle, over planar arrays for applications requiring 360° visibility [10, 11]. In fact, in recent years, ubiquitous radar concepts have been successfully implemented using circular apertures [12].

Despite these obvious advantages, radar systems have been slow to adopt circular apertures and instead accept the limitations offered by the more traditional aperture of a planar array [10]. One reason for this is the ease of design. Planar array design is a straightforward design process often consisting of unit-cell simulations and array factor synthesis. The design process for circular arrays is not quite as simple and straightforward. The geometry of the circular array gives each element in the array a unique pointing direction, which makes each embedded element pattern unique. This further complicates the design of the array by making the synthesis of array tapers and the steering of directional beams more challenging

In recent years, increased interest in the benefits offered by circular/cylindrical apertures has led to increased research and development to mitigate the limitations in their design, implementation, and characterization. The design process for circular/cylindrical arrays is now well-understood, and it is well documented in [13]. The limitations in pattern-synthesis techniques have also become less of a road block as algorithms have been developed for both transmit and receive operation [14]. Phase-only pattern synthesis techniques exist to form omnidirectional transmit patterns with multiple nulls to minimize radiation in desired directions while still maximizing transmit power [15, 16]. On receive, directional patterns with custom sidelobe constraints may be formed [17] and steered [18] over a full 360° in azimuth with no significant degradation to pattern characteristics.

The recent advances in circular array research make it an appropriate time to investigate the development of a radar truly capable of looking *everywhere* at all times – a system truly capable of providing persistent situational awareness. In this report, we compare a cylindrical array to multi-faced planar arrays with an analysis similar to that of Trunk and his colleagues [1–4]. Here, we also demonstrate how such a system might be utilized through an example. A ubiquitous radar system would face additional challenges including range walk, inclusion of acceleration filters to accommodate extended dwell times, and related tracking issues. While significant, those challenges fall outside the scope of this study.

3. Circular Array Overview and Terminology

Before exploring the benefits of a cylindrical array, we begin by defining some key terminology used in the analysis. While the performance of a cylindrical array is intuitive to array designers, there exist some key differences between cylindrical array theory and that of their more commonly used and understood planar counterpart. In this work, we assume that our arrays – both cylindrical and planar – are apertures that can be separated into horizontal and vertical distributions. This allows us to treat our cylindrical array as stacks/tiers of circular arrays. Or, conversely, we view it as a circular array where each element is actual a column of multiple elements. As such, the theory discussed in the remainder of this section focuses on circular arrays.

A circular array consists of N antenna elements having phase centers arranged around a circle of radius R with an angular spacing of $2\pi/N$ between adjacent elements. The N elements in the array are located at spherical coordinates $(R, \pi/2, 2\pi n/N)$ for $n = 0, 1, \ldots, N-1$. Far-field coordinates are defined generically as (r, θ, ϕ). The x-y plane of this configuration is shown in Fig. 1.

Including directional elements in a circular array improves the patterns that are formed at the expense of increased complexity in the synthesis techniques that must be applied [19]. Pattern synthesis for a circular array of directional elements is more involved than for linear or planar arrays since array-factor design techniques are no longer applicable and each embedded element pattern must be included.

The array pattern for the N-element circular can be written generically

$$\vec{F}(\mathbf{k}) = \sum_{n=0}^{N-1} w_n \vec{f}_n(\mathbf{k}) \tag{1}$$

in terms of complex excitation $\{w_n\}$ and complex embedded element patterns $\{\vec{f}_n(\mathbf{k})\}$, which are functions of vector wavenumber $\mathbf{k}$, as discussed in [20]. Each element in the circular array has a unique pointing direction, and thus, all embedded-element patterns are unique. Since the element patterns are related through rotation rather than translation, we are unable to approximate the array pattern as the product of an average embedded element pattern and an array factor. For a circular array, the embedded pattern of each element is related to that of element N, serving here as the prototype, via

$$\vec{f}_n(\mathbf{k}) = \mathbf{R}^n \vec{f}_0(\mathbf{R}^{-n}\mathbf{k}) \tag{2}$$

for some fixed 3×3 rotation matrix $\mathbf{R}$, where $\mathbf{R}$ specifically defines a rotation about the $\hat{z}$-axis. To ensure uniform element distribution and that no elements are duplicated, $\mathbf{R}$ should have the property that $\mathbf{R}^M = \mathbf{I}$ if and only if M is a multiple of N.

Since this study focuses on horizon surveillance, we focus attention to the $\theta = \pi$ plane for the far-field pattern as shown in Fig. 1 and define co-polarized unit-vector $\hat{u}_{co}(\phi)$. While the polarization unit-vectors depend on polar angle ϕ, we suppress this dependence in our nomenclature and use $\hat{u}_{co}$ for simplicity. Using this, we define the co-polarized embedded-element pattern $f(\phi) \triangleq \vec{f(\phi)} \cdot \hat{u_{co}}$ and apply (1) and (2)

$$F(\theta = \pi, \phi) \triangleq F(\phi) = \sum_{n=1}^{N} w_n f_0(\phi - n\frac{2\pi}{N}) \tag{3}$$

to define the pattern in terms of prototype pattern $f_0(\phi)$.

Substituting a Fourier series-domain representation

$$f_n(\phi) = f_0(\phi - n\frac{2\pi}{N}) = \sum_m a_m e^{jm\phi} e^{-j2\pi mn/N}.$$

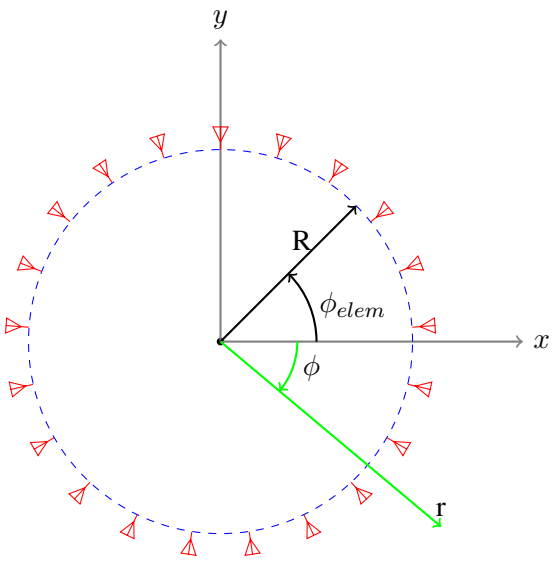

Fig. 1: An N-element circular array of radius R. This diagram shows the array elements and far-field vector.

of the embedded element pattern into (3) yields

$$F(\phi) = \sum_{n=1}^{N} w_n \sum_{m} a_m e^{jm\phi} e^{-j2\pi mn/N}.$$

Now we can replace array excitation vector $\{w_n\}$ with its Fourier series, and the array pattern

$$\begin{aligned} F(\phi) &= \sum_{\ell=0}^{N-1} c_\ell Y_\ell \\ &= \sum_{\ell=0}^{N-1} c_m \sum_{m} a_m \left(\frac{1}{N} \sum_{n=0}^{N-1} e^{j2\pi n(\ell-m)/N} \right) e^{jm\phi} \end{aligned}$$

becomes a weighted summation of IDFT output patterns. Noticing that the term in parenthesis above is equal to 1 only when $(\ell \mod m) = 0$ allows us to replace it with $\delta_{m-\ell-pN}$. Array pattern $F(\phi)$ now becomes

$$\begin{aligned} F(\phi) &= \sum_{\ell=0}^{N-1} c_\ell \sum_{p} \sum_{m} a_m e^{jm\phi} \delta_{m-\ell-pN} \\ &= \sum_{m} a_m c_{m \bmod N} e^{jm\phi}. \end{aligned}$$

We see that by discretely sampling our circular array, we excite harmonics of the desired phase modes often referred to as distortion modes [21].

$$F(\phi) = F_{\text{desired}}(\phi) + F_{\text{dist}}(\phi) \tag{4}$$

where

$$F_{\text{desired}}(\phi) = \sum_{m=0}^{N-1} a_m c_m e^{jm\phi} \tag{5}$$

and where the impact of the distortion modes is contained in

$$F_{\text{dist}} = \sum_{m \notin \{0,\ldots,N-1\}} a_m c_{m \bmod N} e^{jm\phi}. \tag{6}$$

In (5), the desired and distortion patterns are computed as weighted summations of far-field patterns that vary as $e^{jm\phi}$ are referred to as phase mode with order m. The distortion pattern defined in (6) results from the unwanted – but unavoidable – excited harmonics of the desired phase modes.

This discussion shows we can compute/synthesize the array pattern from a circular array using the traditional method of a weighted summation of embedded element patterns using (1). However, we can also compute the pattern in the Fourier-series domain by performing a weighted summation of phase-modes as shown in (4). In the following sections, we show how both domains are used to compute the required radiation patterns for effective ubiquitous radar operation from a circular array.

4. Transmit Patterns

One primary benefit to a radar system offered by a cylindrical array is the convenient reconfiguration of the transmit beam. In standard radar operation, a directional transmit beam can be steered over a full 360° without changes to beamwidth, gain, sidelobe level, or polarization. This is illustrated in Fig. 2 where we compare the azimuth pattern from a single face of a multi-faced planar system to that from an equivalent cylindrical array. To remain consistent with the analysis by Trunk and his colleagues, we define equivalent apertures to have the same number of T/R modules, and thus, the same number of array columns. For these apertures, the arrays have 64 columns of elements operating at 9.0 GHz. The elements in the planar arrays are spaced at $\Delta_M = \frac{\lambda}{1+sin\phi_M}$, where $\phi_M = \frac{\pi}{M}$ defines the maximum scan angle off boresight for the array. In the cylindrical array, we assume a circumferential spacing between elements of $\Delta_C = \frac{\lambda}{2}$ to minimize the impact of distortion modes. This results in a multi-faced planar array system where each face is 10.0 inches long, and a cylindrical array that has a radius of 6.8 inches. For this study, we assume each face of the multi-faced planar systems are square and all cylindrical apertures have the same height as their planar counterpart.

The patterns shown in Fig. 2(c) illustrate benefits of using a cylindrical array for a radar transmitter. In these figures, all elements in the planar array are excited with uniform amplitude and approriate progressive phase ramp to steer the pattern to the desired direction. For the cylindrical array pattern, we excite the same number of elements in one face of the planar array system with phase-only weights $w_m = \frac{f_m^*(\phi_s)}{|f_m^*(\phi_s)|}$ as discussed in [14]. At boresight, the planar array offers 0.97 dB more gain than the cylindrical array. However, as the planar array scans off of boresight, it experiences scan loss from the reduction in projected

aperture size. At the maximum scan angle of 45°, the cylindrical array outperforms the planar array by 2.69 dB in peak gain. To equalize the achievable transmit gain from these two apertures, the planar array would need to be sized significantly larger in order to overcome the scan loss. In transmit arrays, the commonly used figure of merit is ERP. Here, we have used the same number of elements and transmit power for the planar and cylindrical arrays, and thus, the variation in gain is the same as that in ERP.

The concept of ubiquitous radar relies on a broad transmit pattern that illuminates a large scan volume that is be searched continuously with overlapping directional receive beams. A cylindrical array offers wide-ranging flexibility in this regard as the system operates with an omnidirectional radiation pattern to cover a full 360° or wide sector-covering beams if a more restrictive search area is desired. Transmission of an omnidirectional radiation pattern from an appropriately-sampled circular aperture is straightforward. Exciting phase-mode of order m using excitation vector $\mathbf{w} = [w_n] = e^{2\pi mn/N}$ in (1) forms an omnidirectional array pattern for any mode m. For sector-covering beams, we excite (what we refer to here) as *partial phase mode patterns* that use $\mathbf{w} = [w_n] = e^{2\pi mn/N}$ for $m \in M_s$, where M_s defines the sector of excited elements. Elements outside of M_s have $w_n = 0$. This simple approach to forming sector-coverage beams results in beamwidths that approach the width of the angular width of the elements that are excited.

Fig. 3 shows phase mode and partial phase modes – all of order 0. The figure illustrates the ability to control the angular width of the sector illuminated by the transmitter by simply varying the number of elements excited. Here, the full phase mode excites all 64 columns of elements with equal amplitude and phase. For the narrower patterns, sectors of 40 columns, 30 columns, and 20 columns are excited.

Moreover, deeply suppressed null regions are placed in either omnidirectional or sector-coverage beams by applying pattern synthesis techniques included from [15]. This allows the radar to illuminate the entire horizon while nulling out regions where transmission is desired to be avoided. This type of transmission would be more challenging from a multi-faced planar array system.

5. Receive Patterns

On receive, we assume that the system has access to element-level signals and a beamformer capable of forming multiple, simultaneous beams. A pattern-synthesis technique has been developed [17] that optimizes taper loss and sidelobe level – upper bounding one while minimizing the other. Additional work has been done to demonstrate a simple technique for steering any arbitrary cylindrical array excitation in azimuth by transforming it into the Fourier-series domain [18]. These two techniques are illustrated in Fig. 4 where a receive pattern with optimal taper loss is synthesized and scanned throughout the azimuth plane. Inspection of Fig. 4(b) shows minimal – if any – variation in pattern shape as the pattern is steered. We can add upper bounds on sidelobe levels as shown in Fig. 5 where we upper bound the sidelobes to -30 dBp and -40 dBp.

The combination of these techniques allows a radar system to form directional receive beams with reduced sidelobes over a full 360°. Unlike multi-faced planar systems, these receive beams do not vary in beamwidth or sidelobe structure as their steering direction changes.

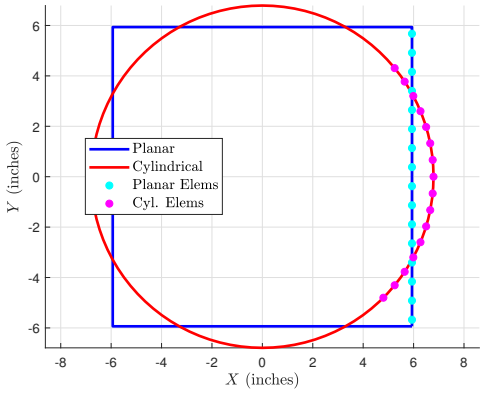

(a) Array layouts showing elements for $\phi = 0^\circ$ scan

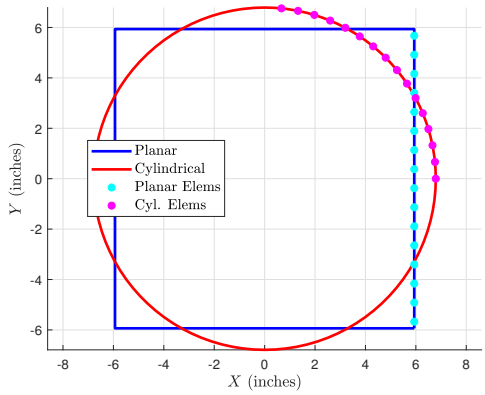

(b) Array layouts showing elements for $\phi = 45^\circ$ scan

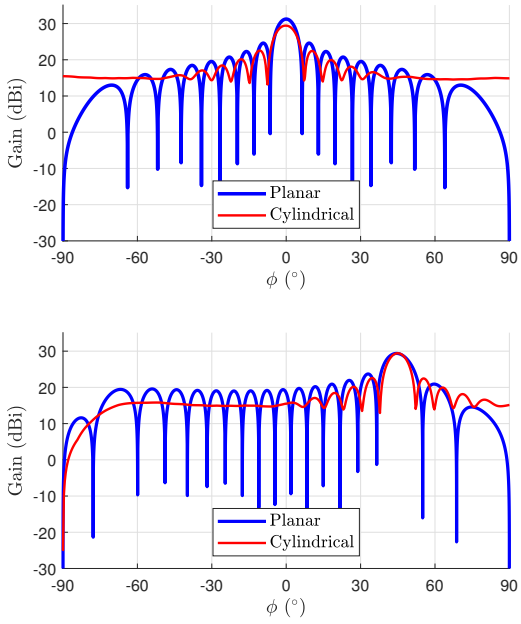

(c) Patterns at boresight and maximum scan angle

Fig. 2: Outline of aperture cross-section for four-faced planar and cylindrical arrays, each having 64 columns of elements along with comparison of the azimuth patterns at broadside and maximum scan position.

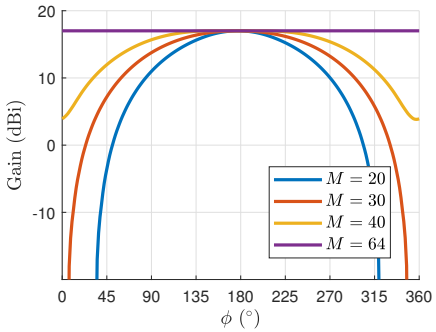

Fig. 3: Sector transmit patterns for the cylindrical array layout shown in Fig. 2(b) as the number of contiguous elements that are excited is varied.

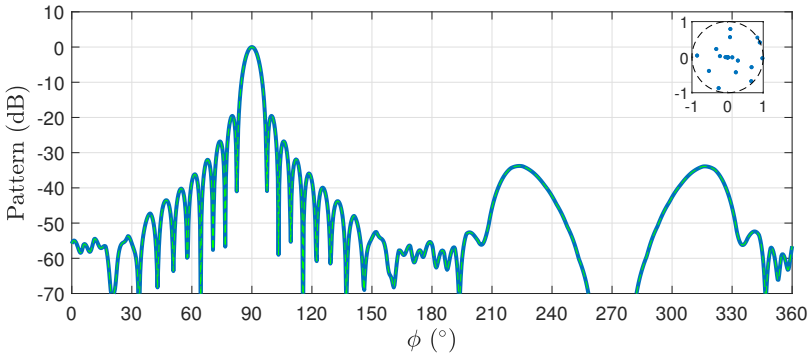

(a) Receive pattern with optimal taper loss

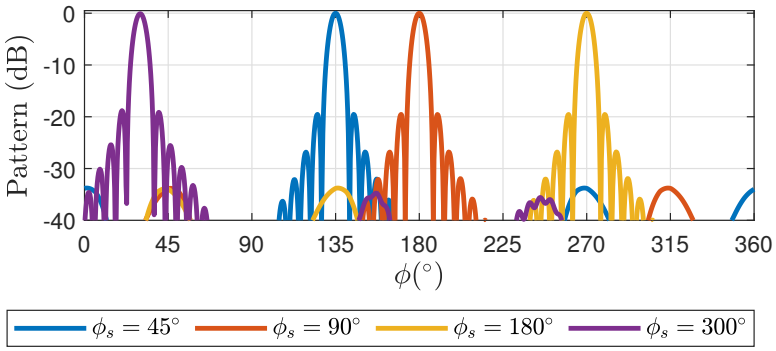

(b) Optimal taper loss pattern scanned to multiple azimuth locations

Fig. 4: Receive patterns synthesized for the array from Fig. 2(b). In (a), the technique from [17] is applied to synthesize a pattern with minimum taper loss, and in (b) we use [18] to steer the beam to multiple locations.

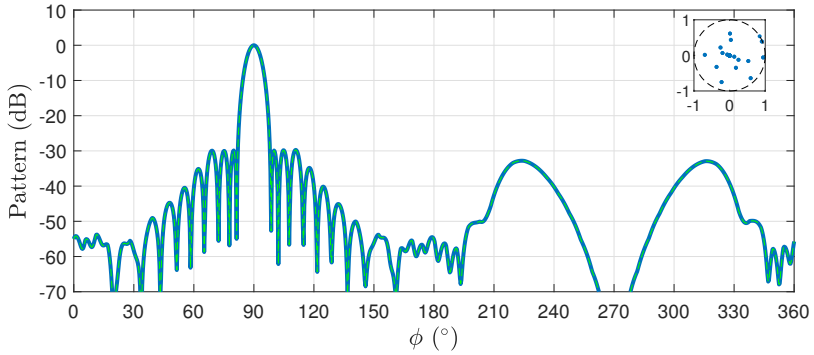

(a) Receive pattern with optimal taper loss and -30 dBp upper bound on sidelobe level

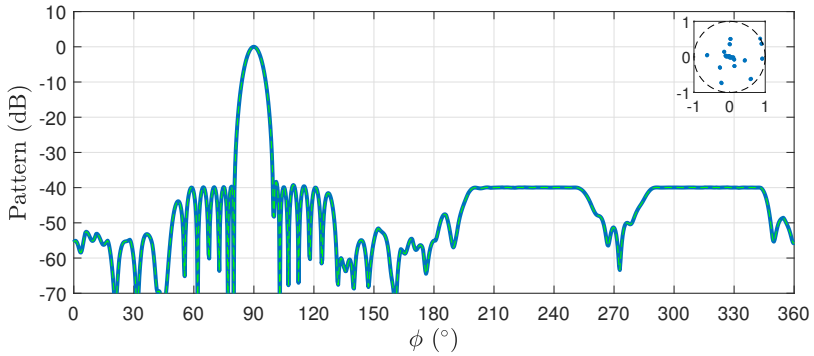

(b) Receive pattern with optimal taper loss and -40 dBp upper bound on sidelobe level

Fig. 5: Receive patterns synthesized for the array from Fig. 2(b). In (a), the technique from [17] is applied to synthesize a pattern with minimum taper loss, and in (b) we use [18] to steer the beam to multiple locations.

6. Radar System Performance: Comparison to Multi-Face Planar Arrays

This section compares horizon search performance offered by a cylindrical phased array to that of a multi-faced planar array system. We follow many of the conventions used by Trunk and Patel in [1, 2, 4] to provide a means of comparison focused on horizon surveillance time assuming a requirement for constant detection range over all beam positions.

The analysis starts by defining the number of faces, M for the multi-faced planar array system and the total number of T/R modules N. As mentioned before, the number of columns per face is $N_m = N/M$, and each array face has $N_m \times N_m$ elements. With M faces, each array face covers an angular sector width of $2\pi/M$, and each array face needs to scan to angles $\pm\pi/M$ off of its boresight direction. This scan requirement dictates the inter-element spacing for the planar array as $\Delta_m = \frac{\lambda}{1+\sin(\pi/M)}$. Finally, the physical length of the planar array face will be $L_m = N_m\Delta_m$.

For the cylindrical array, we assume the same number of T/R modules. The inter-element circumferential spacing is fixed at $\lambda/2$ to minimize the impact of distortion modes while also minimizing the variation in beamshape with scan. Opening up this spacing would provides a larger array size and thus, more gain, but at the expense of more variation with scan and a decreased ability to reduce sidelobe depth. We assume the height of the cylindrical array is the same as the height of the planar array. These definitions provide a parameterized method for comparing multi-faced planar to cylindrical arrays with regards to their performance in horizon surveillance functions.

In this section, we assume that the faces of the multi-faced planar array system operate independently. In order to avoid giving the cylindrical array system an unfair advantage in this study, we limit the number of active elements in the circular array to N/M. This keeps the transmitted power the same for the two apertures and focuses the comparison on the radiation pattern performance with scan of the two aperture concepts.

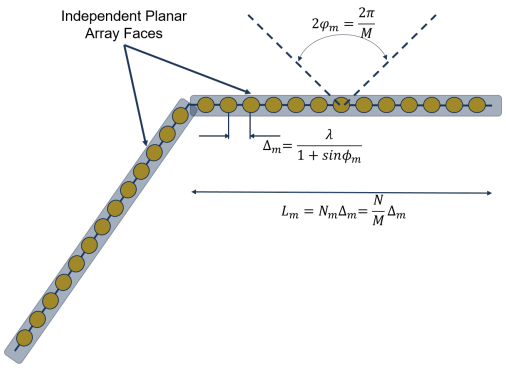

Fig. 6: Definition of parameters for a multi-faced planar array.

6.1 Comparison to a Three-Faced System

Early work by Trunk [1–3] concluded that three faces was the optimal number for a horizon surveillance array system with independent array faces. In this section, we compare the surveillance performance for a three-faced system to a cylindrical system. This study limits the array to 63 columns of elements operating at 9.0 GHz. The layout of the column locations are shown in Fig. 7(a) for the three-faced and cylindrical array systems. Each face of the planar array-based system is 14.25 inches $\times$14.25 inches. The cylindrical array has a radius of 6.79 inches and a height of 14.25 inches.

The azimuth patterns for the two array geometries are compared in Fig. 7(c). The top plot in this figure shows a comparison at boresight, and the bottom compares the gain at $\phi_s = \pi/3 = 60^\circ$. The planar array pattern is computed using uniform excitation with appropriate phase shift assuming the elements have a $\cos^{1.25}\phi$ variation and gain of $\frac{4\pi\Delta_m^2}{\lambda^2}$. The cylindrical array pattern uses the phase-only excitation discussed in Section 4. Scanned cylindrical array patterns are computed using (5). In both sets of patterns, all elements in a given column are excited with uniform amplitude and phase to form a maximum at the horizon. At broadside, the planar array has a larger effective aperture size and consequently, more array gain. However, Fig. 7(b) shows the cylindrical array with a larger effective aperture at the maximum scan angle to illustrate the cylindrical array's ability to avoid scan loss in azimuth. The gain of the planar array relative to the cylindrical array is plotted in Fig. 8(a) as a function of steering angle ϕ_s. The cylindrical array gain exceeds that of the multi-faced planar array system for scan angles $\phi_s > 35^\circ$. In addition to reduced scan loss, Fig. 8 shows another benefit of cylindrical arrays for horizon surveillance. The beamwidth of the cylindrical array remains constant with azimuth scan angle ϕ_s which simplifies scheduling of scan positions.

If we assume that one requirement of the horizon surveillance radar is to maintain constant range at all steering angles, then the decrease in the two-way array gain must be accounted for by increased integration time (dwell time) at each steering angle. We compare array performance by looking at the relative scan time which we define as

$$\tau_{\text{rel}} = \frac{G_{T,\text{cyl}}(\phi_s)G_{R,\text{cyl}}(\phi_s)}{G_{T,\text{p}}(\phi_s)G_{R,\text{p}}(\phi_s)}.$$

Using this expression for relative integration time, we obtain the results of Fig. 8(b). This shows there are modest benefits to the planar array at boresight and small scan angles. However, as scan angles increases beyond 35° the three-faced planar array system requires increased integration time to maintain the desired range. At maximum scan, the three-faced system requires almost four times the integration time of the cylindrical array system.

6.2 Comparison to a Four-Faced System

In [4], Trunk modified his earlier research and arrived at the optimal number of faces being four, rather than the previously determined three. Decreasing the scan range for each face reduces the maximum scan loss and the number of scan positions which, in turn, provides benefits to modern systems. The array layout and pattern comparisons are provided earlier in Fig. 2 including the locations of the elements used for boresight operation and at maximum scan. The relative gain and integration time versus steering angle ϕ_s are shown in Fig. 9. The smaller aperture size leads to a reduction in the boresight advantage of the planar

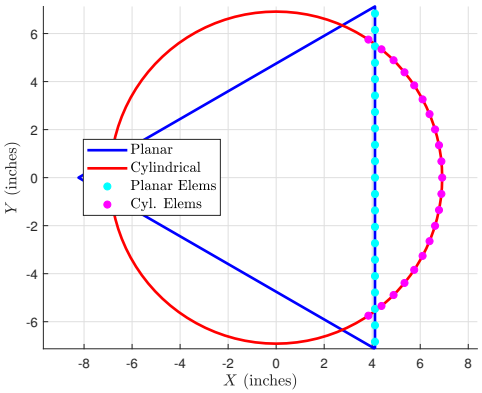

(a) Array Layouts Showing Elements for $\phi = 0^\circ$ scan

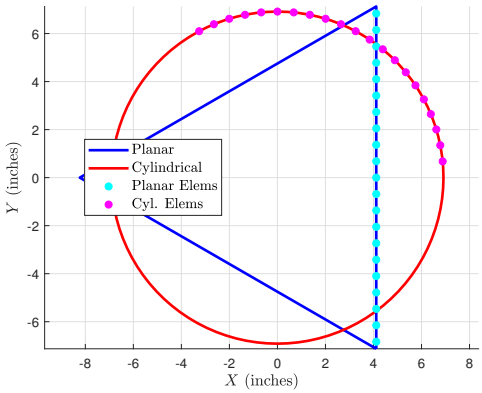

(b) Array Layouts Showing Elements for $\phi = 60^\circ$ scan

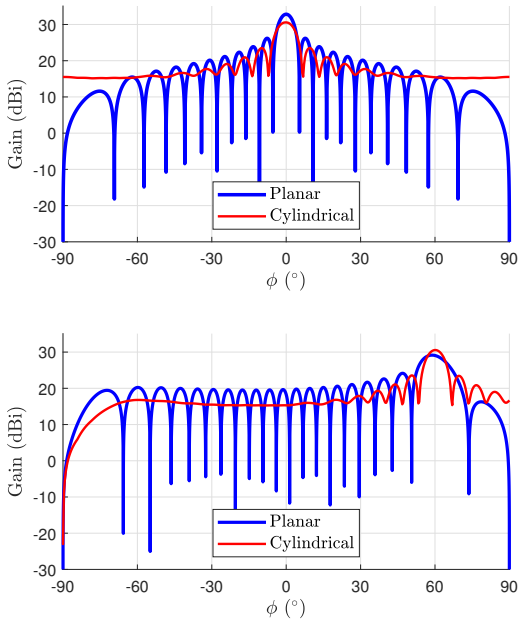

(c) Patterns at boresight and Maximum Scan Angle

Fig. 7: Outline of aperture cross-section for three-faced planar and cylindrical arrays, each having 64 columns of elements along with comparison of the azimuth patterns at broadside and maximum scan position.

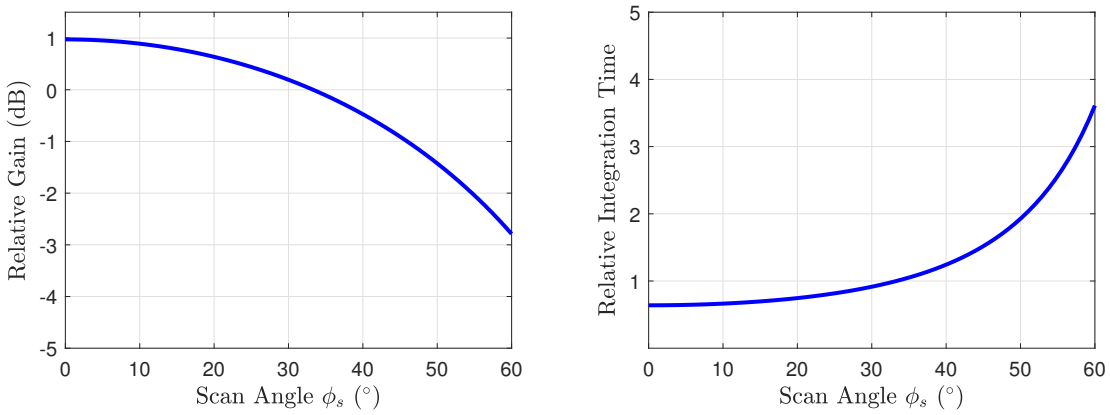

(a) Relative Gain (b) Relative Integration Time

Fig. 8: Relative gain and integration time over a sector for a face of the three-faced array system to a cylindrical array-based system.

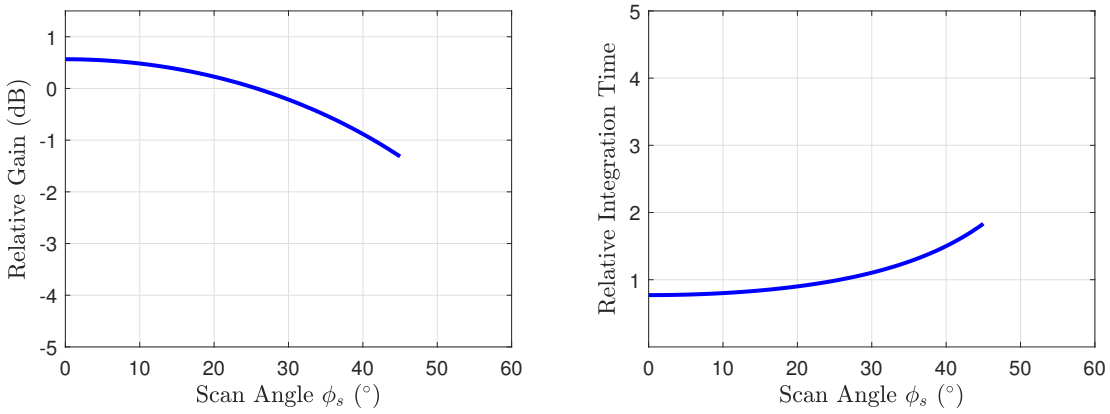

(a) Relative Gain (b) Relative Integration Time

Fig. 9: Relative gain and integration time over a sector for a face of the four-faced array system to a cylindrical array-based system.

array system at boresight then for the three-faced system. The limited scan requirements also reduce the integration time increase at the maximum scan angle.

7. Impact of Coherently Using Faces of Multi-Faced System: Polygonalized Arrays

Section 6.1 and Section 6.2 show cylindrical arrays provide benefits over multi-faced arrays for horizon surveillance radar primarily because of the elimination of scan loss. However, cylindrical arrays have some drawbacks that limit their integration onto certain platforms. The cylindrical geometry complicates integration of T/R modules behind the array while providing a geometry more complex to manufacture than standard planar panels, and the cylindrical geometry potentially has undesirable impact on radar cross section (RCS).

In this section, we explore array geometries that are a compromise between multi-faced planar and cylindrical geometries: *polygonalized arrays*. Here, by polygonalized designs, we are discussing a faceted version of a cylindrical array, where N/M of the array elements are contained on a potentially small planar array face [22], and we assume that elements are used coherently regardless of the face they are a part of. The goal of such a design is to enable cylindrical array performance from a geometry that could potentially ease manufacturing and T/R module integration by replacing the curvilinear structure. This array system is only applicable if a system is able to use multiple faces coherently and approaches a true cylindrical array in the limit as $M \to N$.

From a system perspective, we make a few assumptions. First, we assume that the receive system digitizes at the element level and has the processing capability to tile the azimuth plane with overlapping beams. Secondly, we assume the system has N_{Tx} transmitters, thus allowing it to simultaneously form N_{Tx} transmit beams with N/N_{Tx} transmit elements contributing to each beam. We specify the number of faces M only to define the geometry, but that is all. Elements on any array face can contribute to the transmit and receive beams. We also limit element spacing on the multi-faced planar array to $\lambda/2$ to allow elements on several faces to contribute with beamforming similar to that used in cylindrical arrays. Smaller array faces no longer mean simply reducing the scan requirements of a face, as the array-face gain reduces significantly for large M. Instead, we are merely approximating a cylinder having circular cross-section with one of an M-sided polygon.

As an example, we modify our previous four-faced array system to allow coherent use of elements on all faces. The transmit side is still limited to N/M columns at a time, but these elements can now span multiple faces to mitigate scan loss. On receive, we use all elements. This provides significant benefit in terms of integration time as shown in Fig. 10(c). Further improvements are obtained by increasing the number of faces for the polygonalized array.

We compare the performance of the cases outlined in Fig. 11. Each of these cases has 64 columns, and each column contains 16 elements. The 64 columns are divided among 4, 8, 16, 32, and 64 faces. We note that the case of 64 faces is a true cylindrical array. Fig. 12(a) shows transmit gain as a function of scan angle ϕ_s for the polygonalized arrays. All transmit patterns use the 16 elements with closest $\phi_n = \text{atan}(y_n/x_n)$ to ϕ_s. Not surprisingly, the results show reduced ripple as the number of faces increases at the expense of reduced peak gain. On receive, all of the elements are used for all cases. This results in the receive gain plot of Fig. 12(b) showing higher gain than the transmit case with reduced ripple as a function of ϕ_s. Again, we see that the ripple decreases as the number of array faces increases. The combined transmit-receive gain is shown in Fig. 12(c). The cylindrical array case ($M = 64$) shows the least ripple with respect to ϕ_s. However, the other cases show that polygonalized arrays provide similar performance even for small number of faces.

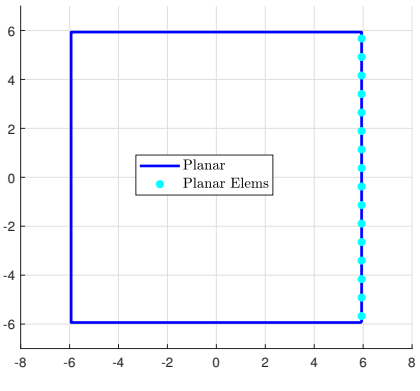

(a) Independent faces geometry

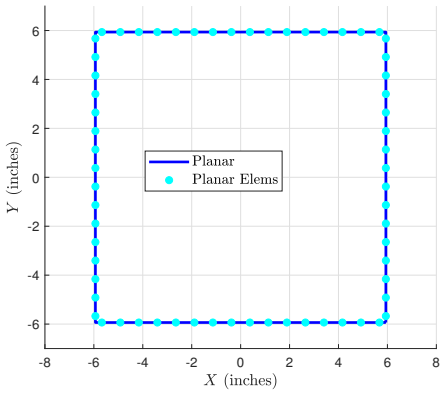

(b) Polygonalized array geometry (coherent faces)

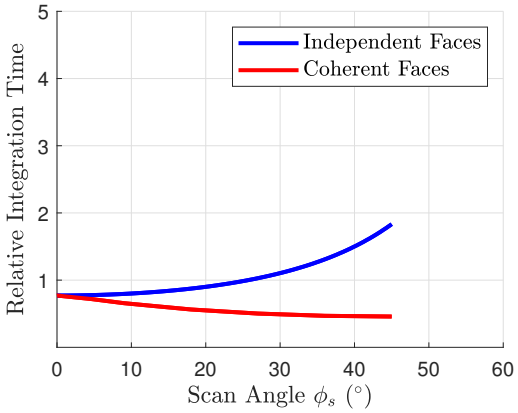

(c) Relative integration time

Fig. 10: Relative integration time over a traditional four-faced array and a polygonalized four-face array system where all faces are used coherently.

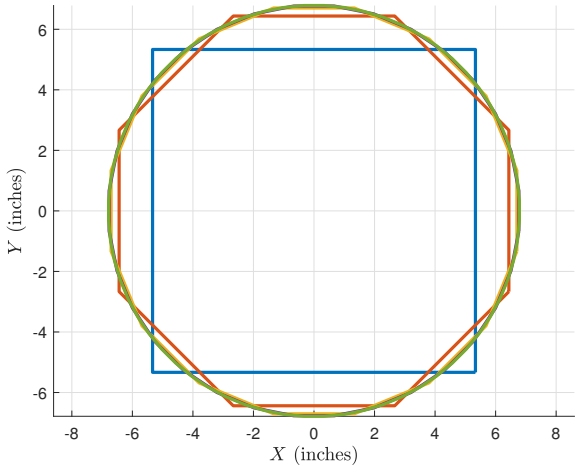

Fig. 11: Array layouts for polygonalized 64-column arrays of multiple array-face sizes .

8. Application of Polygonalized Arrays to Ubiquitous Radar

In addition to a reduction in scan loss that provides surveillance time benefits to a horizon search radar, polygonalized arrays also have the transmit-pattern flexibility that enables many of the concepts of ubiquitous radar. The ability to transmit over a full 360° in azimuth while tiling the azimuth plane with overlapping receive beams – potentially with reduced sidelobes – make rapid horizon surveillance a possibility. In this section, we provide an example of surveillance radar operation from a cylindrical array with discussion of both advantages and disadvantages.

Performing ubiquitous radar from a polygonalized array would include transmission of an omnidirectional pattern. For horizon search, this most likely means all elements in a given column are excited to form peak gain at the horizon, and the columns of the array are fed with a waveform using a linear phase progression to account for the deviation from the element locations on the polygonalized array faces to a circular aperture. In the limit as $M \rightarrow N$, this excitation becomes a phase-mode of order 0. This pattern clearly has reduced gain compared to directional transmit patterns because we have eliminated any gain from the azimuth beamforming. However, that gain reduction is at least partially offset in ERP by the increased transmit power obtained from utilizing all elements in the array simultaneously for transmit. Transmit ERP for the directional and omnidirectional modes are shown in Fig. 13 assuming transmit power of 1 W per array column. The directional mode in this example has $12dB$ more gain than the omnidirectional. Since it uses all elements in the array, the omnidirectional case has 6 dB more transmit power. This results in 6 dB more ERP from the directional mode compared to the omnidirectional case.

As a comparison point, we look at performing traditional horizon surveillance from a cylindrical array. Directional receive beams and transmit beams are steered in unison to desired beam positions through the azimuth plane. This technique has the benefit of increased gain and ERP, which reduces dwell time for a given detection range.

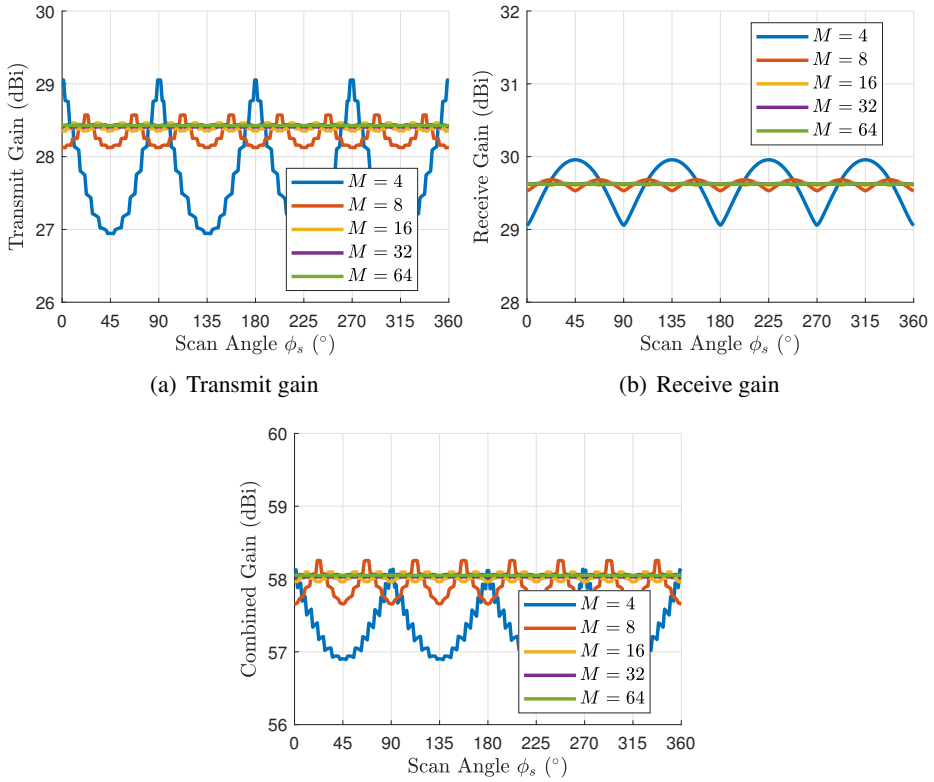

(a) Transmit gain

(b) Receive gain

(c) Combined gain

Fig. 12: (Top) transmit gain, (middle) receive gain, and (bottom) combined gain for the polygonalized array geometries shown in Fig. 11. 16 columns of elements are used on transmit and all are used on receive.

To compare dwell times, we define the metric

$$\tau_d = \frac{1}{P_{Tx} G_{Tx} G_{Rx}}$$

that is a function of transmit power P_{Tx}, transmit gain G_{Tx}, and receive gain G_{Rx}. Fig. 14(a) plots

$$\tau_r \triangleq \frac{\tau_d}{\tau_{d0}}$$

which is a normalization of the dwell times to a baseline value τ_{d0}. In this case, the baseline value is that of the $M = 4$ case when $\phi = 0$. If we constrain the system to provide constant detection range, then there is a ripple in dwell time that is inversely proportional to the ERP results from Fig. 13(a). The magnitude of the ripple decreases as the number of faces increases. The corresponding scan time metric $\tau_s = N_{\text{pos}} \tau_d$ is then the product of the dwell-time metric and the number of required scan positions for the transmit beam N_{pos}. For the ubiquitous radar case, $N_{\text{pos}} = 1$. For the directional transmit mode, the radar needs to form transmit beams that most likely overlap at their 3 dB points. For this example, the receive beamwidth for

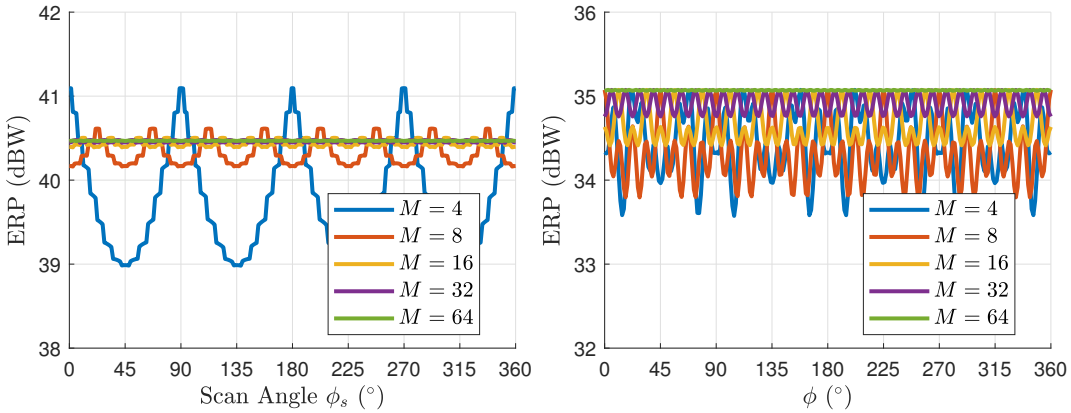

(a) Scanned directional patterns

(b) Omnidirectional pattern

Fig. 13: ERP for directional mode and omnidirectional mode transmitters using polygonalized arrays. Directional mode is plotted as a function of steering angle.

the cylindrical array is $7.2°$ requiting 50 transmit positions. Because we assume 4 transmitters, we can form 4 simultaneous transmit beams. Consequently, $\tau_s = 12.5\tau_d$. The relative dwell times for directional mode and omnidirectional (ubiquitous) modes are plotted in Fig. 14 along with overall surveillance scan time. The ubiquitous array system has noticeable improvements in search time compared to the directional-beam radar system. However, in order to realize this benefit, the radar system must be able to handle the increased dwell times.

The patterns for the ubiquitous and directional radar cases are shown in Fig. 15 for the cylindrical array case ($M = 64$). We assume that there are 50 beam positions to ensure receive beams overlap at their 3 dB points. The receive beam dictates scan positions since it has the narrower beam pattern. The receive beams are the same for both the directional and ubiquitous radar cases. However, the transmit patterns for the two cases differ. Fig. 15(a) shows overlapping directional transmit patterns as well as an omnidirectional pattern. The omnidirectional pattern has 12 dB less gain than the directional transmit patterns, but it has 6 dB more transmit power. Thus, this plot shows a net 6 dB reduction in ERP for the omnidirectional transmit pattern compared to that of the directional case.

Additional patterns are shown in Fig. 16 where an omnidirectional transmit pattern is overlaid with 50 directional receive patterns. We show directional receive patterns with -40 dB sidelobes obtained using the technique from [17] and steered using [18]. These patterns can be compared to those of Fig. 17 for a traditional horizon surveillance radar where transmit and receive beams are steered in unison. These two examples use the same transmit beams as in Fig. 15, but have receive patterns with reduced sidelobes.

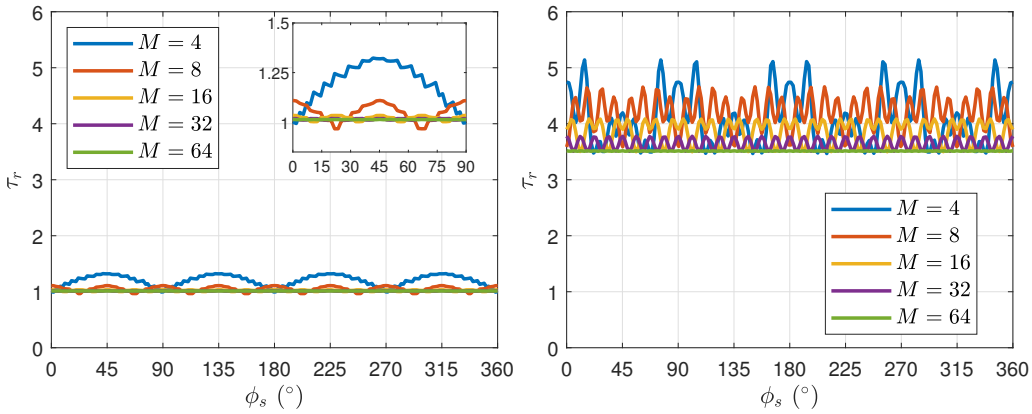

(a) Directional mode dwell time

(b) Omnidirectional mode time

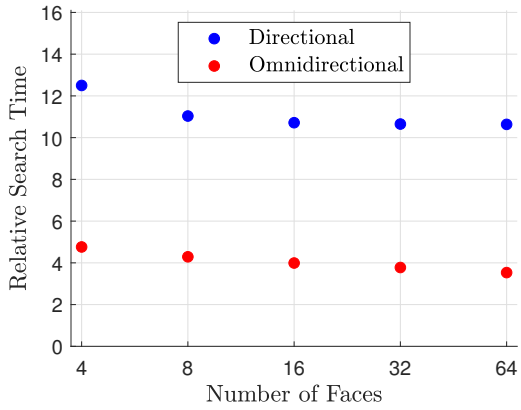

(c) Relative search times

Fig. 14: Relative dwell times and horizon search time for directional and omnidirectional mode radars using polygonalized arrays with various number of faces.

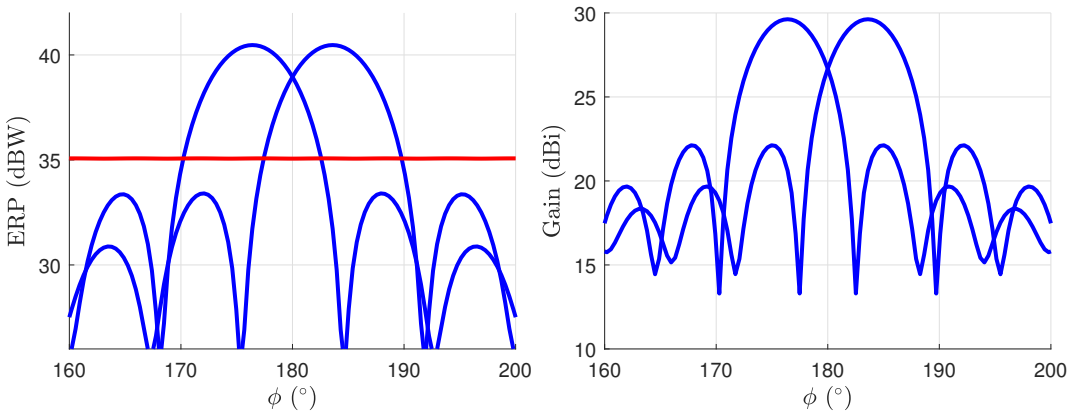

(a) Transmit patterns

(b) Receive patterns

Fig. 15: Transmit and receive patterns for the 64-column cylindrical array ($M = 64$) of the example from Fig. 14. The receive patterns are overlapping at their 3 dB points. The transmit pattern assumes 1 W per element and have patterns overlapping at the 3 dB points of the receive pattern as well as the omnidirectional pattern used for the ubiquitous radar application.

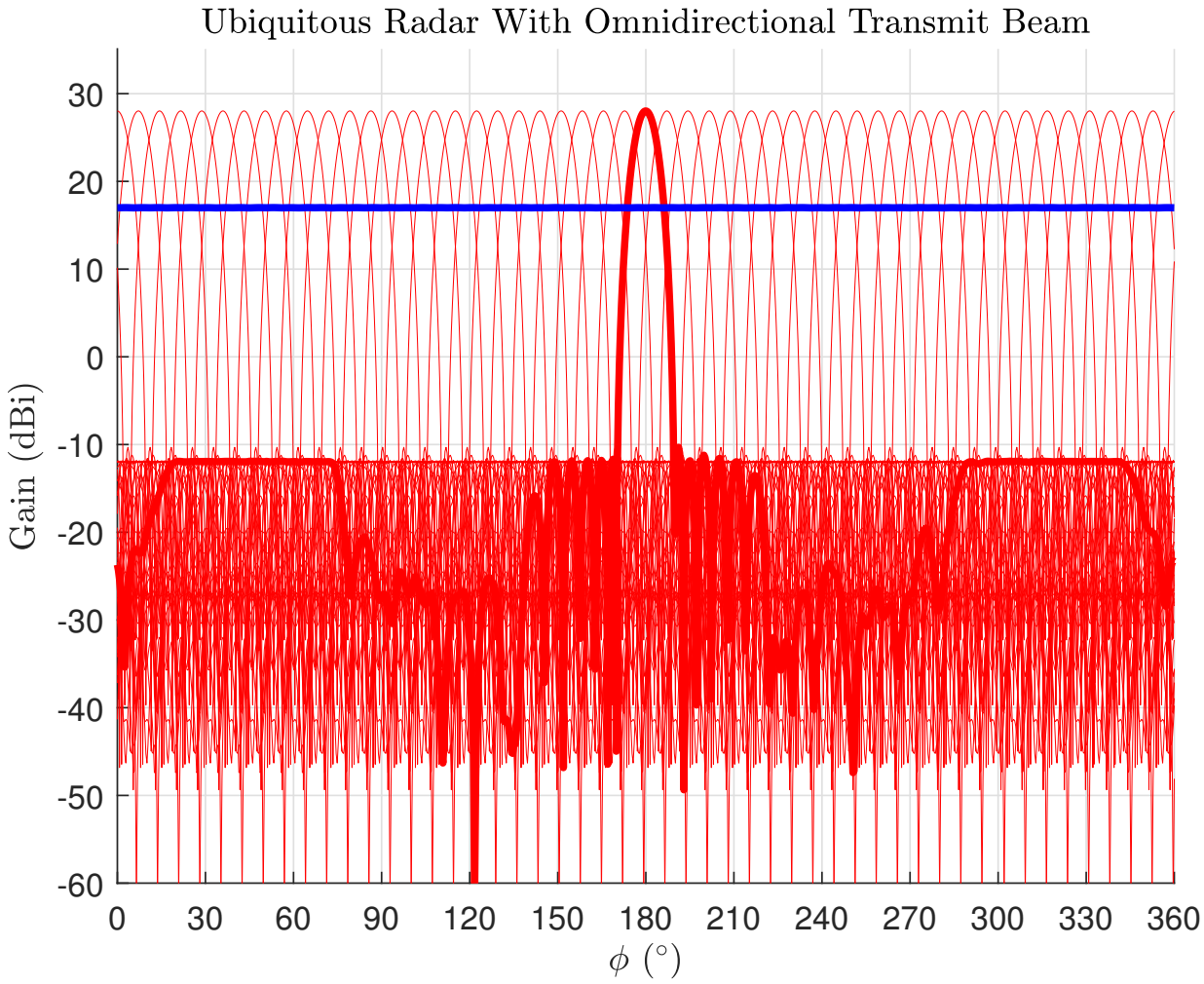

Fig. 16: Omnidirectional transmit pattern and overlapping low-sidelobe receive patterns for executing ubiquitous radar from a cylindrical phased array.

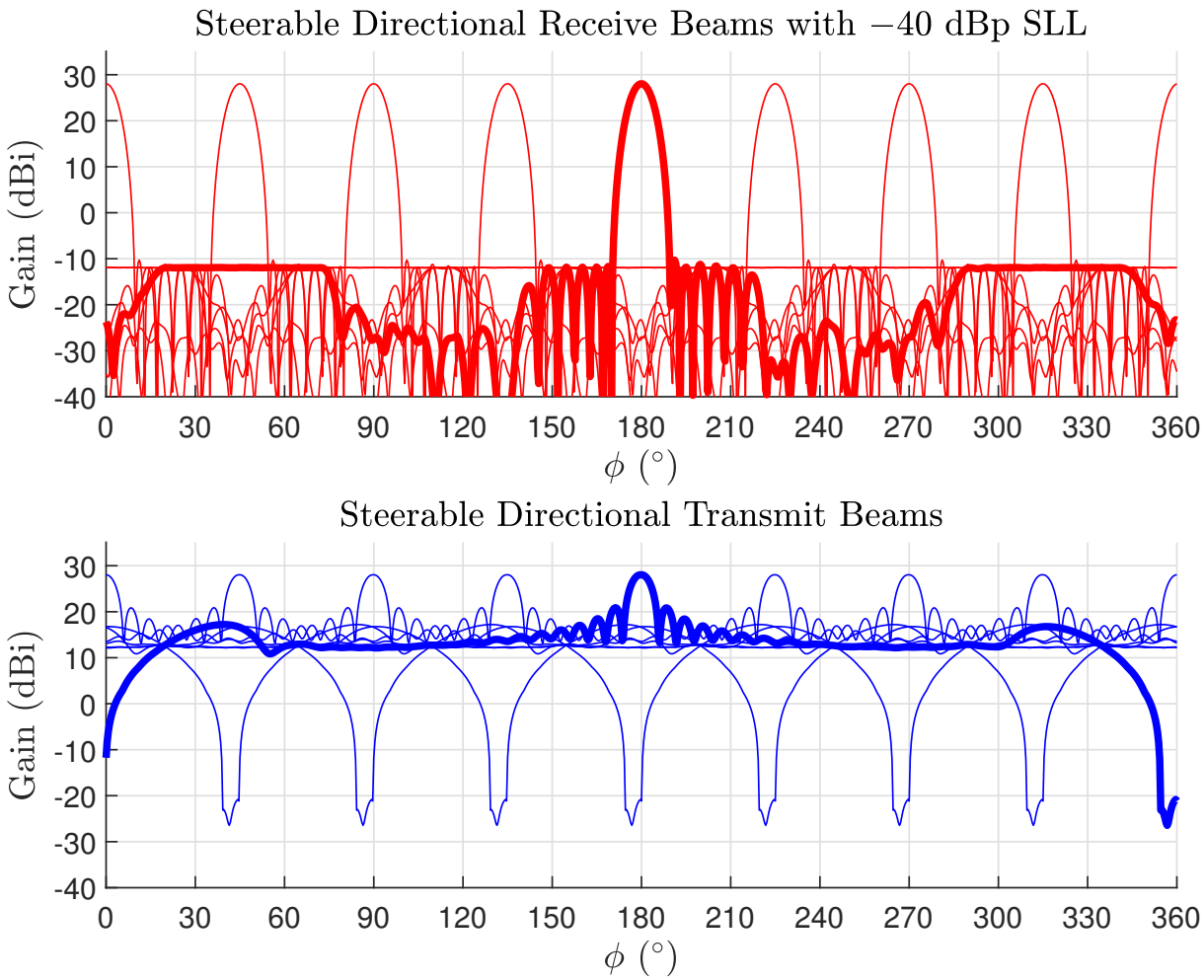

Fig. 17: (Top) Steerable low-sidelobe receive patterns and (bottom) steerable directional transmit patterns for executing horizon surveillance radar from a cylindrical phased array.

9. Conclusions

Cylindrical phased arrays offer benefits for surveillance radars stemming from their inherent azimuthal symmetry and instantaneous visibilty of a full 360°. These apertures have been shown to have obvious benefits over multi-faced planar arrays – at least in the traditional manner in which multi-faced planar arrays are used. Cylindrical arrays form directional beams that scan throughout the azimuth plane with constant gain, beamwidth, sidelobe structure, and polarization. They also conveniently form broad sector-covering and omnidirectional transmit patterns, which enable the application of ubiquitous radar techniques. Polygonalized phased arrays provide a compromise between planar arrays and cylindrical arrays that improves surveillance performance. The form factor allows application of traditional array design techniques while simplifying the integration of supporting electronics modules. Coherent operation of the array faces allows the polygonalized array to approach the radiation pattern performance of a cylindrical array.

Cylindrical and polygonalized arrays improve surveillance performance compared to traditional multi-faced planar array systems. Omnidirectional transmit patterns improve search times, at the expense of either reduced range or increased dwell times. The radar can also switch to a traditional search using directional beams to extend range and reduce dwell time. All of this reconfiguration is accomplished electronically, with no mechanical steering required.

REFERENCES

1. G. V. Trunk and D. P. Patel, "Optimal number of phased array faces for horizon surveillance," in *International Symposium on Phased Array Systems and Tech.*, 1996, pp. 214–216.

2. ——, "Optimal number of phased array faces and signal processors for horizon surveillance," *IEEE Trans. on Aerospace and Electronic Systems*, vol. 33, no. 3, pp. 1002–1006, 1997.

3. W. M. Waters, D. P. Patel, and G. V. Trunk, "Optimum number of faces of a volume-scanning active array radar," *IEEE Trans. on Aerospace and Electronic Systems*, vol. 34, no. 3, pp. 1032–1037, 1998.

4. G. V. Trunk, "Optimal number of phased array faces for horizon and volume surveillance revisited," in *IEEE International Symposium on Phased Array Systems and Tech.*, 2003, pp. 124–129.

5. J. J. Alter, R. M. White, F. F. Kretschmer, I. D. Olin, and C. L. Temes, "Ubiquitous radar: an implementation concept," in *IEEE Radar Conference*, April 2004, pp. 65–70.

6. M. Skolnik, "Role of radar in microwaves," *IEEE Transactions on Microwave Theory and Techniques*, vol. 50, no. 3, pp. 625–632, Mar 2002.

7. J. O. Coleman and W. M. Dorsey, "Phase-only beam broadening in large transmit arrays using complex-weight gradient descent," in *IEEE International Symp. on Phased Array Systems and Tech.*, Oct 2013, pp. 440–447.

8. D. P. Scholnik, "A parameterized pattern-error objective for large-scale phase-only array pattern design," *IEEE Trans. Antennas Propag.*, vol. 64, no. 1, pp. 89–98, Jan 2016.

9. W. M. Dorsey and D. P. Scholnik, "A hybrid global-local optimization approach to phase-only array-pattern synthesis," in *IEEE Radar Conference*, May 2015, pp. 1417–1422.

10. G. Galati, F. Madia, P. Carta, E. G. Piracci, R. Stallone, and M. Massardo, "Time for a change in phased array radar architectures - part i: Planar vs. conformal arrays," in *2015 16th International Radar Symposium (IRS)*, June 2015, pp. 912–917.

11. G. Galati, F. Madia, P. Carta, E. G. Piracci, S. Franco, and S. Quattrociocchi, "Time for a change in phased array radar architectures- part ii: The d-radar," in *2015 16th International Radar Symposium (IRS)*, June 2015, pp. 918–923.

12. P. Carta, G. Galati, E. G. Piracci, F. Madia, and R. Ronconi, "Implementation of the ubiquitous radar concept with a conformal array," in *2015 European Radar Conference (EuRAD)*, Sept 2015, pp. 441–444.

13. C. J. Fulton and A. Mirkamali, "A computer-aided technique for the analysis of embedded element patterns of cylindrical arrays [em programmer's notebook]," *IEEE Antennas and Propagation Magazine*, vol. 57, no. 3, pp. 132–138, June 2015.

14. W. M. Dorsey and D. P. Scholnik, "Transmit and receive circular array pattern synthesis for radar applications," in *IEEE Radar Conference*, May 2016, pp. 1–6.

15. W. M. Dorsey, R. Mital, and D. P. Scholnik, "Phase-only synthesis of omnidirectional patterns with multiple nulls from a uniform circular array," in *IEEE International Symp. on Antennas and Propag.*, June 2016, pp. 765–766.

16. D. P. Scholnik and W. M. Dorsey, "Transmit pattern synthesis for uniform circular arrays with active reflection constraints," in *IEEE Radar Conference*, May 2017, pp. 1562–1567.

17. W. M. Dorsey, J. O. Coleman, and W. R. Pickles, "Uniform circular array pattern synthesis using second-order cone programming," *IET Microwaves, Antennas Propagation*, vol. 9, no. 8, pp. 723–727, 2015.

18. J. O. Coleman and W. M. Dorsey, "Phase-shift steer a uniform circular array in the fourier-series domain," in *Wireless and Microwave Technology Conference (WAMICON)*, April 2017, pp. 1–4.

19. T. Rahim and D. Davies, "Effect of directional elements on the directional response of circular antenna arrays," *IEE Proc. on Microwaves, Optics and Antennas*, vol. 129, no. 1, pp. 18–22, February 1982.

20. D. Kelley and W. Stutzman, "Array antenna pattern modeling methods that include mutual coupling effects," *IEEE Trans. Antennas Propag.*, vol. 41, no. 12, pp. 1625–1632, 1993.

21. L. Josefsson and P. Persson, *Conformal Array Antenna Theory and Design*, ser. IEEE Press Series on Electromagnetic Wave Theory. Wiley, 2006. [Online]. Available: https://books.google.com/books?id=MQXZDm9IVyEC

22. G. H. Huff, K. White, D. Grayson, F. Espinal, W. M. Dorsey, and A. Stumme, "Polygonalization of mm-wave dual-band circular phased arrays for multi-mode beamforming," in *Wireless and Microwave Technology Conference (WAMICON)*, 2018, pp. 1–4.